Title

Simultaneous control of magnetic topologies for reconfigurable vortex arrays

Journal

NPG Asia Materials, 9(2)

ISSN

1884-4049

Authors

Im, Mi-Young
Fischer, Peter
Han, Hee-Sung
et al.

Publication Date

2017-02-01

DOI

10.1038/am.2016.199

Peer reviewed

Simultaneous control of magnetic topologies for reconfigurable vortex arrays

Mi-Young Im[1,2*], *Peter Fischer*[3,4], *Hee-Sung Han*[5], *Andreas Vogel*[6], *Min-Seung Jung*[2], *Weilun Chao*[1], *Young-Sang Yu*[7], *Guido Meier*[6,8,9], *Jung-Il Hong*[2*], *and Ki-Suk Lee*[5*]

[1]Center for X-ray Optics, Lawrence Berkeley National Laboratory, Berkeley CA94720, USA

[2]Department of Emerging Materials Science, DGIST, Daegu, Korea

[3]Materials Sciences Division, Lawrence Berkeley National Laboratory, Berkeley CA 94720, USA

[4]Department of Physics, University of Santa Cruz, CA 94056, USA

[5]School of Materials Science and Engineering, KIST-UNIST Ulsan Center for Convergent Materials, Ulsan National Institute of Science and Technology, Ulsan, Korea

[6]Institut für Angewandte Physik und Zentrum für Mikrostrukturforschung, Universität Hamburg, Jungiusstrasse 11, 20355 Hamburg, Germany

[7]Advanced Light Source, Lawrence Berkeley National Laboratory, Berkeley CA94720, USA

[8]The Hamburg Centre for Ultrafast Imaging, 22761 Hamburg, Germany

[9]Max-Planck Institute for the Structure and Dynamics of Matter, Luruper Chaussee 149, 22761 Hamburg, Germany

*Corresponding Authors : Mi-Young Im (mim@lbl.gov), Jung-Il Hong (jihong@dgist.ac.kr), Ki-Suk Lee (kisuk@unist.ac.kr)

ABSTRACT

Magnetic vortices in confined magnetic elements have drawn enormous attentions owing to their fascinating topological textures offering a platform for understanding the fundamental physics of nanoscale spin behavior and in view of harnessing their unique spin structures for advanced magnetic technologies. For magnetic vortices to be practical, an effective reconfigurability of the two topologies of magnetic vortices, i.e. the circularity and the polarity, is an essential prerequisite. The reconfiguration issue is highly relevant to the question of whether both circularity and polarity are reliably and efficiently controllable or not. Here, we report the first direct observation for the simultaneous control of both circularity and polarity by application only of an in-plane magnetic field to arrays of asymmetrically shaped permalloy disks. Our investigation demonstrates that the high degree of reliability for the control of both topologies can be achieved by tailoring the geometry of disk arrays. We also propose a new approach to control vortex structures by manipulating the effect of stray field on the dynamics of vortex creation. Present study is expected to pave the way for complete and effective reconfiguration of magnetic vortex structures, thereby enhancing the prospect for the technological applications of magnetic vortices.

'

KEYWORDS: Nanospin texture, Magnetic vortex, X-ray microscopy, Nanodisks, Micromagnetic simulation

INTRODUCTION

Magnetic vortex in a micronsized ferromagnetic element consists of the central core (polarity, p) that points out-of-plane either up (p = +1) or down (p = -1) and the in-plane magnetization (circularity, c) rotates around the core either clockwise (c = +1, CW) or counter-clockwise (c = -1, CCW). Since both circularity and polarity can be specified by two independent values, i.e. c = ±1 and p = ±1, four distinct spin states can exist in a single magnetic element with the combination of circularity and polarity. Magnetic vortices have been intensively studied due not only to their compelling physical behavior[3-7] but also to their potentials in a wide range of applications such as data storage,[8,9] signal transfer,[10-12] logic devices,[13] transistors,[14] and artificial skyrmion crystals.[15-18] With respect to the realization of magnetic vortices' practical application in advanced nanotechnologies, one of the critical factors is the effective reconfigurability of two topologies, c and p, particularly within large and densely packed arrays of magnetic elements.[19,20] As a representative example, for successfully achievement of vortex-based signal transfer as well as the logic and transistor operations, desired configurations of magnetic vortex states need to be established first.[10-14] And, uniformly arranged vortex structures are also essentially required to generate artificial skyrmion crystals based on magnetic vortices in proximity to perpendicularly magnetized thin films.[15-18]

For effective reconfiguration of magnetic vortex structures, one of the key issues is the reliable and efficient control of both c and p in magnetic vortices. It is also vital for their storage application. So far, both static and dynamic studies on the control of vortex structures have mostly been dedicated to the manipulation of either c or p alone.[8,21-31] Few attempts have been made for the control of both c and p, but they have been carried out without repetition, meaning that only single event of control has been investigated.[32,33] Therefore, the reliability and

repeatability for the control of both topological features has not yet been addressed. In addition, multiple manipulating methods, e.g. both in-plane and out-of-plane magnetic fields, have been applied to achieve the control of both *c* and *p*. The reliable control of both *c* and *p* with the application of single control factor, such as either in-plane or out-of-plane field, as well as in-depth understanding of relevant physics remain challenges as yet.

In the present investigation, we demonstrate that the application of an in-plane magnetic field alone enables simultaneous control of *c* and *p* in the array of asymmetric permalloy (Py, $Ni_{80}Fe_{20}$) disks with one flat-edge side. The reliability in the control of vortex structures is found to be sensitively dependent on the geometry of nanodisk arrays such as the flat-edge ratio (*r*, as defined in Figure 1) and the disk height (*h*). Based on a comprehensive understanding of the stray field effect on the dynamic process of vortex creation, we propose a new means of vortex-state control that makes possible global and/or local reconfiguration of vortex structures in closely packed permalloy disks.

MATERIALS AND METHODS

Sample preparation

Py disk arrays were fabricated by e-beam lithography and sequential lift-off processes on X-ray transparent silicon-nitride membranes. The disk radius (*R*) and interdisk distance (*d*) were fixed as R = 500 nm and d = 200 nm, while the disk height (*h)* and flat-edge ratio (*r)* were varied from h = 40nm to 100 nm and from $r = 0.1R$ to $0.2R$.

Imaging of magnetic vortex structures

To observe complete vortex structures (i.e. both circularity and polarity), we employed, at the Advanced Light Source (XM-1, beamline 6.1.2.),[34] magnetic full-field transmission soft X-ray

microscopy (MTXM). In-plane and out-of-plane magnetizations were imaged by mounting the specimens at 60º and 90º angles with respect to the incident X-ray beam direction, respectively. The magnetic contrast at XM-1 is provided by an X-ray magnetic circular dichroism (XMCD) mechanism. The X-ray beam energy was set at Fe L_3 edge (707 eV) of the X-ray absorption spectra. To enhance the magnetic contrast and to eliminate any non-magnetic background, the images taken in the remanent state were normalized by a reference image imaged in the saturation state. To saturate the Py disks, an in-plane magnetic field of +100 mT or -100 mT was applied parallel to the flat edge of disks shown in Fig. 1.

Micromagnetic simulations

Micromagnetic simulations were conducted with disks of $2R$ = 999 nm, h = 40 nm, r = 99 nm (~ 0.2R), and the interdisk distance of d = 201 nm, which dimensions are almost identical to those of disks ($2R$ = 1000 nm, h = 40 nm, r = 100 nm (~ 0.2R), and d = 200 nm) studied in the experiments. The lateral dimensions of the disks and interdisk distance were multiples of 3 nm owing to the cell size, 3 × 3 × 5 nm^3, chosen for the simulations. The micromagnetic simulations were carried out using the object-oriented micromagnetic framework (OOMMF) code,[35] which numerically solves the Landau-Lifshitz-Gilbert equation[36,37] for the local magnetization vector **M(r, *t*):** $\partial \mathbf{M}/\partial t = -\gamma(\mathbf{M}\times\mathbf{H}_{eff}) + (\alpha/|\mathbf{M}|)(\mathbf{M}\times\partial\mathbf{M}/\partial t)$ with the phenomenological damping constant $\boldsymbol{\alpha}$, the gyromagnetic ratio γ, and the effective field $\mathbf{H}_{eff}$. The standard material parameters for Py were used: saturation magnetization M_s = 800 kA/m, exchange stiffness A_{ex} = 13 pJ/m, damping constant α = 0.01, and zero magnetocrystalline anisotropy. Periodic boundary conditions was utilized in the simulations so as to be able to take account of stray fields induced by adjacent disks within the arrays of disks.

RESULTS AND DISCUSSION

Direct observation of magnetic vortex structures

Figure 1 shows the schematic diagram of a Py disk array with a radius of R = 500 nm, a height of h = 100 nm, an interdisk distance of d = 200 nm, and a flat-edge ratio of $r = 0.2R$. The creation of vortex structures in the disk array was achieved by a positive field sequence: the magnetic field of +100 mT is applied in the positive x direction ($H = +H_x$) parallel to the flat edges of disk elements to fully saturate the disks and then they are relaxed to the remanent state at 0 mT by turning off the magnetic field. The insert in Fig. 1 illustrates MTXM images of in-plane spin configurations observed in the array after the positive field sequence. The direction of magnetization in the disk plane is indicated by a white arrow. The in-plane magnetic contrast allows the value of c to be determined. It is clearly evident that with the positive field sequence, the preferably created circularity is CCW(c = -1). To determine if there is any field-direction effect on the type of created circularity, we also observed vortex structures formed after the sequence: applying the field of -100 mT in the negative x direction ($H = -H_x$) and turning off the field to 0 mT (hereafter, negative field sequence). In Figure 2a, we show representative series of images for the in-plane domain structures taken from two different field sequences in the disk arrays with the edge ratio of $r = 0.1R$ and $r = 0.2R$. In both arrays, a CW (c = +1) circularity is created as a result by the negative field sequence while CCW (c = -1) circularity forms in the positive field sequence. This shows that by altering the direction of the in-plane field, circularity can be selectively created in the asymmetric disks. It should be noted that the rotational sense of circularity selected by each field sequence in disks within the array shown in Fig. 2a is opposite to the one formed in an isolated disk with the identical field sequence.[24,26,27] Under the positive (negative) field sequence, CCW (CW) circularity is generated in disks within the array, whereas

CW (CCW) circularity is created in an isolated disk.[24,26,27] To understand the change in the type of created circularity between disks within the array and a single isolated disk, we considered the effect of stray field on vortex creation process. Based on micromagnetic simulations for vortex formation with and without considering stray field, we confirmed that the dynamics of vortex creation can be considerably changed by stray field. Under the influence of stray field, the dynamic process of vortex formation in the positive (negative) field sequence proceeds toward for the creation of CCW (CW) circularity as observed in disks within the array (Fig. 2a). The detailed dynamic procedure and the stray field effect on the dynamics will be discussed later.

Controllability of circularity in asymmetric disk arrays

Next, the reliability of circularity-control (controllability) was quantitatively investigated by switching the direction of external field for various arrays of disks with different disk heights and flat-edge ratios, as shown in Figure 2b. To accumulate statistically meaningful data, the experimental procedure schematized in Figure 2a was repeated 40 times and vortex structures in 25 individual disks were examined in each array. As the metric for controllability, the generation rate of an identical circularity in any given disk within 40 repetitions was counted; the controllability is defined as 1 (0) if the generation rate of CCW circularity is 100 % (50 %) within 40 repeated cycles with the positive field sequence (for which CCW circularity is predominantly generated). In Figure 2b, the error bar represents the standard deviation of controllability over the 25 disks. It is noteworthy that reliability for the formation of vortex structure with the same circularity in asymmetric disks is certainly improved in comparison with the case of symmetric circular disks. The reliability of circularity-control is above 95 % in asymmetric disks with h = 100 nm, as seen in Fig. 2b, while probability for the formation of vortex structures with the same circularity determined from statistical measurements (20

repetitions, 25 individual disks) is lower than 35 % in the case of symmetric full disks with the same height of 100 nm. In Fig.2b, we find that controllability is sensitive to the geometry of disk arrays. As the flat-edge ratio increases from $r = 0.1R$ to $0.2R$, controllability increases and the disks of h = 100 nm show higher controllability than do those of h = 40 or 70 nm. The high controllability of more than 0.9 observed in the 100 nm thick disks regardless of the edge ratio might be due to the less pronounced impact of thermal fluctuations associated with the large volume of disks. Indeed, thermal fluctuation[39] is an inherent factor hindering reliable control of magnetic processes.[40,41] The intensity of thermal fluctuation is in inverse proportion to an activation volume, which is related to the thermal effect.[42] In the vortex formation, disk volume could be considered as an activation volume[43] since the formation process accompanies with multiple steps of nucleation and annihilation of vortex and antivortex over the whole disk not only the vortex core.[38] The effective thermal effect is reduced by the factor of 2.5 as the disk height increases from 40 nm to 100 nm. That is, the disks of h = 100 nm are less prone to thermal fluctuations than are thinner disks; consequently, in larger-volume disks, the same type of vortex structure can be more reliably created.

Simultaneous control of circularity and polarity in asymmetric disks

In disks of h = 100 nm and $r = 0.2R$, which exhibit an approximate 97% accuracy in circularity-control, we verified the simultaneous control of c and p through direct imaging of circularity and polarity. Figure 3a shows MTXM images of in-plane and out-of-plane magnetic structures observed in an identical region of the array. In the out-of-plane MTXM images, the white and black spots in the centers of the disks indicate down and up polarities, respectively. Remarkably, the change of field-direction triggers a switching of not only the circularity but also the polarity. A CW circularity (c = +1) with a down polarity (p = -1) is formed after the positive field

sequence, whereas a CCW circularity (c = -1) with an up polarity (p = +1) most often is generated after the negative field sequence. A simplified illustration of this observed phenomenon is provided in Figure 3b. The results indicate that simultaneous control of c and p is feasible by a single manipulation process, which is to say, the application of an in-plane magnetic field in the asymmetric disks. This suggests the possibility of highly efficient reconfiguration of magnetic-vortex structures in nanodisk arrays. Our result is very unexpected and intriguing, since only c has been considered to be controllable in asymmetric disks.[24-28] The simultaneous control of c and p is thought to be related to the asymmetric nature in the formation process of vortex states, reported in our previous work.[7] It was found that two different vortex state groups with cp = +1 and cp = -1 are not energetically equivalent in a single circular disk due to both intrinsic and extrinsic factors. Either cp = +1 or cp = -1 is more stable than the other and the energetically favored vortex group dominantly forms. In the case of asymmetric disks (Figure 3a), cp = -1 is more favored than cp = +1. If c = +1 switches to c = -1, p tends to flip from p = -1 to p = +1 in order to form cp = -1. Notably, c and p are not independent, but they are linked with each other that c and p tend to switch together. This intrinsic connection between c and p would be a critical feature that needs to be seriously considered for individual control of c and p. Circularity in asymmetric disks, unlike circular disks, is controllable by altering the direction of the magnetic field, which allows for simultaneous control of c and p in such disks. The reliability of the simultaneous control of c and p, as determined by a statistical ensemble of 300 events (15 repetitions, 20 individual disks), was found to be 0.77 ± 0.17 and 0.79 ± 0.16 in 100 nm thick disks of 0.2R and 0.1R edge ratio, respectively. The errors correspond to the standard deviations of reliability for the 20 disks. It should be noted that the data obtained from the statistical ensemble covers any possible randomness or imperfection of vortex control that

can exist in some of disks as shown in one of the six disks in the lower-middle panel and two of the six disks in the lower-right panel, as indicated by white dots in Fig. 3 (a). The reliability of vortex control can differ from one disk to another, mainly due to randomly generated surface-related extrinsic factors such as roughness and defects. It is expected that the accuracy of the control of both *c* and *p* can be further enhanced by optimizing geometries of asymmetric disk arrays.

New approach for the control of vortex structures in asymmetric disks

Finally, we propose a new way to control *c* in asymmetrically shaped disks. Since, as demonstrated in Figure 3, simultaneous control of *c* and *p* is feasible when *c* is reliably controlled, this method could replace the one involving alteration of the direction of an in-plane field for control of both *c* and *p* in asymmetric disks. As noted with respect to Figure 2, the stray field is the critical magnetic factor for the determination of finally formed *c* states in asymmetric disks, as it significantly affects the dynamics at the early stage of vortex formation process.[38] A certain type of circularity, ether of $c = +1$ or $c = -1$, is selected, according to whether the stray field exists or not. Our approach to the control of *c* is to manipulate the stray field effect on the dynamic process of vortex creation using an additional, static and uniform field (hereafter, the control field). The control field can create an effective stray field environment of closely packed disks into an isolated disk and vice versa.

First, to fully understand the influence of stray field on the process of vortex structure formation, micromagnetic simulations of the dynamics of vortex formation in an isolated element and the same element with neighboring identical elements have been performed without taking into account the control field. The two disks were set to the exactly same geometry of $2R = 999$ nm, $h = 40$ nm, $r = 99$ nm ($\sim 0.2R$), and the interdisk distance of $d = 201$ nm, which parameters are

almost equal to those ($2R$ = 1000 nm, h = 40 nm, r = 100 nm (~ 0.2R), and d = 200 nm) of disk studied in experiments. Figure 4a shows images of simulated dynamic processes in an isolated single disk (upper) and in a disk within the array of d = 201 nm (lower). The color on the disk surface represents the curl of in-plane magnetization (m); the red (blue) color indicates the CCW (CW) winding direction of m and the arrow indicates the direction of in-plane magnetization on the disk surface. To trigger vortex creation, the disks were initially saturated by +100 mT and then relaxed to 0 mT within τ = 4.4 ns. The strength of stray field generated in the disk array of d = 201 nm during the process was estimated to be about 10 mT in the +x direction. In the early stage of vortex formation (≤ 7.2 ns for isolated disks (upper), ≤ 9.7 ns for a disk within an array (lower)), almost identical dynamic processes were observed in the two disks: two vortices are injected from the left and right sides of disk, respectively, and they move closer to each other. Since they have the same CCW circularity (red), a cusp-shaped magnetization configuration is formed between them and is transformed into an oxbow-shaped configuration (t = 11.6 ns (upper) and 12. 3 ns (lower)). As the dynamics progressed, an additional CW vortex appeared (t = 12.1 ns (upper) and 15. 4 ns (lower)). The effect of the stray field becomes obvious from the comparison of the isolated disk at t = 14 ns (upper) with the disk within the array at 15. 8 ns (lower). In the isolated disk, the initially injected CCW vortices move toward the flat edge of the disk while the newly created CW vortex (blue) is located in the central region. However, due to the stray field in the disk within the array of d = 201 nm, the two CCW vortices remain at the center while the CW vortex is annihilated at the round edge. Consequently, in the isolated disk, inner-disk CW vortex becomes the final vortex structure, whereas in the disk within the array, one of the initially injected CCW vortices survives as the ultimate vortex. So, in summary, the

stray field in the d = 201 nm (~10 mT) array stimulates the creation of CCW circularity in the positive field sequence from +100 mT to 0 mT.

To clarify our concept of circularity-control using a control field, we again conducted micromagnetic simulations in identical systems. The disks were relaxed to 0 mT from the fully saturated state at +100 mT, according to the procedure outlined in Figure 4a. However, in this simulation, control fields of ±10 mT were additionally applied at the moment the 100 mT saturation field was turned off. By turning on the control field of +10 mT (-10 mT) in the positive field sequence, the saturation field of +100 mT reduces directly to +10 mT (-10 mT). The purpose of control field is to make for an environment similar to that in which stray field exists in an isolated disk and to create the condition under which there is no stray field in the disk within the array by countervailing the influence of the stray field induced by adjacent disks within the array. The control-field strength (10 mT) was chosen based on the results shown in Figure 4a, in which case, the stray field in the disk array of d = 201 nm was about 10 mT. The direction of the control field was set as + x for the isolated disk and -x for the disk within the array, considering the fact that the stray field in the array of d = 201 nm was in the +x direction (Figure 4a). Snapshot images taken from the simulations are displayed in Figure 4b. The dynamics in the isolated disk with the applied +10 mT control field (upper) are analogous to that observed in the disk within the array (Figure 4a). The initially injected CCW vortices (red) shift to the center of the disk during the annihilation of the CW vortex (blue) at the 16.4 ns stage, and consequently, the final vortex, as in the case of the disk within the d = 201 nm array with no control field (Figure 4a), is CCW. Meanwhile, the dynamic process in the disk within the array with the induced -10 mT control field (lower) was almost identical to that witnessed in the isolated disk (Figure 4a). The CW vortex newly created at the 12.2 ns stage is located in the

middle of the disk with the two CCW circularities pushed toward the edge (13.6 ns) and the CW vortex finally forms. The simulation results support that the effect of stray field on the dynamic process of vortex creation can be manipulated by the applied control field and the finally created vortex structure is consequently controlled.

This proposed approach was also confirmed experimentally. Fig. 5 shows series of images for in-plane domain structures observed in an isolated disk (a) and in disks within array of d =200 nm after their relaxation from the saturation to the remanent state without and with applying the control field of +30 mT and -30 mT, respectively. The positive value of H_{control} was applied to an isolated disk for mimicking the stray field exists in arrays and the negative value of H_{control} was applied to disks within the array for compensating the effect of stray field induced by adjacent disks. We applied H_{control} with the same external field magnet used for the saturation of disks. To reproduce the procedure done in simulations, H_{control} was applied immediately after the saturation field of +100 mT was turned off and then finally created vortex structures were observed after turning off H_{control}. Within three repeated measurements, as shown in Fig. 5, it is notable that by applying H_{control} during the formation process of vortex structure, the created circularity switches from CW (c = 1) to CCW (c = -1) in the isolated disk and CCW (c = -1) to CW (c = 1) in disks within the array although few exceptions could also be observed occasionally, which is in good agreement with simulation results. In experiment, H_{control} stronger than 10 mT was preferred to reliably manipulate the stray field effect. It is thought that the stray field from neighboring disks in the array may not exactly be 10 mT but exceed 10 mT in real samples with nonideal geometries. We also found that reliability for the control of vortex structure utilizing H_{control} is improved as the strength of control field increases. Based on 20 repeated measurements, it was verified that reliability for the control of circularity can be greater than 80 % with

$H_{control}$ = ±50mT. In this way, for both an isolated disk and a disk within an array, the circularity can be simply controlled by turning on or off the additional $H_{control}$ without any need to alter any aspects of array geometry such as interdisk distance. This method, moreover, offers the possibility of selective control of specific vortex structures in closely packed disks with simple electrode architecture, thereby also enabling, in disk arrays, local reconfiguration of magnetic vortices. By applying current through an electrode during the relaxation of disks from the saturation state to remanence, circularity is controllable by means of an Oersted field thus generated. The Oersted field induces a control-field effect equal to that shown in Figure 4b and Figure 5, which latter field can control the stray field from adjacent disks within arrays. Any type of electrode is applicable, though the field generated must be strong enough to offset the effect of the stray field that already exists within arrays.

CONCLUSION

We report herein that the simultaneous control of vortex circularity and polarity can be achieved by a simple procedure entailing application of an in-plane magnetic field and the reliability of which approach can be enhanced with optimized geometry of asymmetric disk arrays. In light of the fact that reliable and simultaneous control of *c* and *p* could be crucially beneficial to realize the effective reconfiguration of magnetic vortex structures within arrays, this work may bring forward the possibility for the applications of magnetic vortices to advanced magnetic nanotechnologies.

CONFLICT OF INTEREST

The authors declare no conflict of interest.

ACKNOWLEDGMENT

This work was supported by Leading Foreign Research Institute Recruitment Program through the National Research Foundation (NRF) of Korea funded by the Ministry of Education, Science and Technology (MEST) (2012K1A4A3053565, 2014R1A2A2A01003709, and 2015M3D1A1070465), and by the KIST-UNIST partnership program (2V03870/2V03880) and equivalently by the 2014 Research Fund (1.140019.01) of UNIST (Ulsan National Institute of Science and Technology). Work at the ALS was supported by the Director, Office of Science, Office of Basic Energy Sciences, Scientific User Facilities Division of the U.S. Department of Energy under Contract No. DE-AC02-05CH11231. P.F. acknowledges support by the Director, Office of Science, Office of Basic Energy Sciences, Materials Sciences and Engineering Division of the U.S. Department of Energy under Contract No. DE-AC02-05CH11231 within the Non-Equilibrium Magnetic Materials Program. A.V. and G.M. acknowledge financial support from the Deutsche Forschungsgemeinschaft via SFB 668 “Magnetism from the Single Atom to the Nanostructure” and via Graduiertenkolleg 1286 “Functional Metal-Semiconductor Hybrid Systems”.

REFERENCES

1. Shinjo, T., Okuno, T., Hassdorf, R., Shigeto, K. & Ono, T. Magnetic Vortex Core Observation in Circular Dots of Permalloy. *Science* **289**, 930-932 (2000).
2. Wachowiak, A., Wiebe, J., Bode, M., Pietzsch, O., Morgenstern, M. & Wiesendanger, R. Direct Observation of Internal Spin Structure of Magnetic Vortex Cores. *Science* **298**, 577-580 (2002).
3. Tanigaki, T., Takahashi, Y., Shimakura, T., Akashi, T., Tsuneta, R., Sugawara, A. & Shindo, D. Three-dimensional observation of magnetic vortex cores in stacked ferromagnetic discs. *Nano. Lett.* **15**, 1309-1314 (2015).
4. Fischer, P., Im, M.-Y., Kasai, S., Yamada, K., Ono, T. & Thiaville, A. X-ray imaging of vortex cores in confined magnetic structures. *Phys. Rev. B* **83**, 212402 (2011).
5. Adolff, C.F., Hänze, M., Pues, M., Weigand, M. & Meier, G. Gyrational modes of benzenelike magnetic vortex molecules. *Phys. Rev. B* **92**, 024426 (2015).
6. Behncke, C., Hänze, M., Adolff, C.F., Weigand, M. & Meier, G. Band structure engineering of two-dimensional magnonic vortex crystals. *Phys. Rev. B* **91**, 224417 (2015).
7. Im, M.-Y., Fischer, P., Yamada, K., Sato, T., Kasai, S., Nakatani, Y. & Ono, T. Symmetry breaking in the formation of magnetic vortex states in a permalloy nanodisk. *Nat. Commun.* **3**, 983 (2012).
8. Van Waeyenberge, B., Puzic, A., Stoll, H., Chou, K.W., Tyliszczak, T., Hertel, R., Fahnle, M., Bruckl, H., Rott, K., Reiss, G., Neudecker, I., Weiss, D., Back, C.H. & Schutz, G. Magnetic vortex core reversal by excitation with short bursts of an alternating field. *Nature* **444**, 461-464 (2006).
9. Mitin, D., Nissen, D., Schädlich, P., Arekapudi, S.S.P.K. & Albrecht, M. Single vortex core recording in a magnetic vortex lattice. *J. Appl. Phys.* **115**, 063906 (2014).
10. Han, D.S., Vogel, A., Jung, H., Lee, K.S., Weigand, M., Stoll, H., Schutz, G., Fischer, P., Meier, G. & Kim, S.K. Wave modes of collective vortex gyration in dipolar-coupled-dot-array magnonic crystals. *Sci. Rep.* **3**, 2262 (2013).
11. Sugimoto, S., Fukuma, Y., Kasai, S., Kimura, T., Barman, A. & Otani, Y. Dynamics of coupled vortices in a pair of ferromagnetic disks. *Phys. Rev. Lett.* **106**, 197203 (2011).

12. Vogel, A., Kamionka, T., Martens, M., Drews, A., Chou, K.W., Tyliszczak, T., Stoll, H., Van Waeyenberge, B. & Meier, G. Coupled vortex oscillations in spatially separated permalloy squares. *Phys. Rev. Lett.* **106**, 137201 (2011).
13. Jung, H., Choi, Y.-S., Lee, K.-S., Han, D.-S., Yu, Y.-S., Im, M.-Y., Fischer, P. & Kim, S.-K. Logic Operations Based on Magnetic-Vortex-State Networks. *ACS Nano* **6**, 3712-3717 (2012).
14. Kumar, D., Barman, S. & Barman, A. Magnetic vortex based transistor operations. *Sci. Rep.* **4**, 4108 (2014).
15. Sun, L., Cao, R.X., Miao, B.F., Feng, Z., You, B., Wu, D., Zhang, W., Hu, A. & Ding, H.F. Creating an artificial two-dimensional Skyrmion crystal by nanopatterning. *Phys. Rev. Lett.* **110**, 167201 (2013).
16. Gilbert, D.A., Maranville, B.B., Balk, A.L., Kirby, B.J., Fischer, P., Pierce, D.T., Unguris, J., Borchers, J.A. & Liu, K. Realization of ground-state artificial skyrmion lattices at room temperature. *Nat. Commun.* **6**, 8462 (2015).
17. Miao, B.F., Sun, L., Wu, Y.W., Tao, X.D., Xiong, X., Wen, Y., Cao, R.X., Wang, P., Wu, D., Zhan, Q.F., You, B., Du, J., Li, R.W. & Ding, H.F. Experimental realization of two-dimensional artificial skyrmion crystals at room temperature. *Phys. Rev. B* **90**, 174411 (2014).
18. Li, J., Tan, A., Moon, K.W., Doran, A., Marcus, M.A., Young, A.T., Arenholz, E., Ma, S., Yang, R.F., Hwang, C. & Qiu, Z.Q. Tailoring the topology of an artificial magnetic skyrmion. *Nat. Commun.* **5**, 4704 (2014).
19. Streubel, R., Kronast, F., Rößler, U.K., Schmidt, O.G. & Makarov, D. Reconfigurable large-area magnetic vortex circulation patterns. *Phys. Rev. B* **92**, 104431 (2015).
20. Martín, J.I., Vélez, M., Hoffmann, A., Schuller, I.K. & Vicent, J.L. Artificially Induced Reconfiguration of the Vortex Lattice by Arrays of Magnetic Dots. *Phys. Rev. Lett.* **83**, 1022 (1999).
21. Hertel, R., Gliga, S., Fahnle, M. & Schneider, C.M. Ultrafast nanomagnetic toggle switching of vortex cores. *Phys. Rev. Lett.* **98**, 117201 (2007).
22. Yu, Y.-S., Lee, K.-S., Jung, H., Choi, Y.-S., Yoo, M.-W., Han, D.-S., Im, M.-Y., Fischer, P. & Kim, S.-K. Polarization-selective vortex-core switching by tailored orthogonal Gaussian-pulse currents. *Phys. Rev. B* **83**, 174429 (2011).

23. Bohlens, S., Krüger, B., Drews, A., Bolte, M., Meier, G. & Pfannkuche, D. Current controlled random-access memory based on magnetic vortex handedness. *Appl. Phys. Lett.* **93**, 142508 (2008).
24. Kimura, T., Otani, Y., Masaki, H., Ishida, T., Antos, R. & Shibata, J. Vortex motion in chilarity-controlled pair of magnetic disks. *Appl. Phys. Lett.* **90**, 132501 (2007).
25. Huang, L., Schofield, M.A. & Zhu, Y. Control of double-vortex domain configurations in a shape-engineered trilayer nanomagnet system. *Adv. Mater.* **22**, 492-495 (2010).
26. Wu, K.-M., Horng, L., Wang, J.-F., Wu, J.-C., Wu, Y.-H. & Lee, C.-M. Influence of asymmetry on vortex nucleation and annihilation in submicroscaled permalloy disk array. *Appl. Phys. Lett.* **92**, 262507 (2008).
27. Schneider, M., Hoffmann, H. & Zweck, J. Magnetic switching of single vortex permalloy elements. *Appl. Phys. Lett.* **79**, 3113 (2001).
28. Dumas, R.K., Gilbert, D.A., Eibagi, N. & Liu, K. Chirality control via double vortices in asymmetric Co dots. *Phys. Rev. B* **83,** 060415 (2011).
29. Giesen, F., Podbielski, J., Botters, B. & Grundler, D. Vortex circulation control in large arrays of asymmetric magnetic rings. *Phys. Rev. B* **75**, 184428 (2007).
30. Haldar, A. & Adeyeye, A.O. Vortex chirality control in circular disks using dipole-coupled nanomagnets. *Appl. Phys. Lett.* **106**, 032404 (2015).
31. Uhlir, V., Urbanek, M., Hladik, L., Spousta, J., Im, M.Y., Fischer, P., Eibagi, N., Kan, J.J., Fullerton, E.E. & Sikola, T. Dynamic switching of the spin circulation in tapered magnetic nanodisks. *Nat. Nanotechnol.* **8**, 341-346 (2013).
32. Jaafar, M., Yanes, R., Perez de Lara, D., Chubykalo-Fesenko, O., Asenjo, A., Gonzalez, E.M., Anguita, J.V., Vazquez, M. & Vicent, J.L. Control of the chirality and polarity of magnetic vortices in triangular nanodots. *Phys. Rev. B* **81,** 054439 (2010).
33. Shimon, G., Ravichandar, V., Adeyeye, A.O. & Ross, C.A. Simultaneous control of vortex polarity and chirality in thickness-modulated [Co/Pd]n/Ti/Ni80Fe20 disks. *Appl. Phys. Lett.* **105**, 152408 (2014).
34. Fischer, P., Kim, D.-H., Chao, W., Liddle, J.A., Anderson, E.H. & Attwood, D.T. Soft X-ray microscopy of nanomagnetism. *Mater. Today* **9**, 26-33 (2006).
35. Donahue, M. J. & Porter, D. G. *OOMMF User's Guide Version 1.0 Interagency Report NISTIR 6376*, National Institute of Standards and Technology: Gaitherburg, MD, (1999).

36. Landau, L. D. & Lifshitz, E. M. Theory of the dispersion of magnetic permeability in ferromagnetic bodies. *Phys. Z. Sowjetunion* **8**, 153 (1935)

37. Gilbert, T.L. A phenomenological theory of damping in ferromagnetic materials. *IEEE Trans. Magn.* **40**, 3443-3449 (2004).

38. Im, M.-Y., Lee, K.-S., Vogel, A., Hong, J.-I., Meier, G. & Fischer, P. Stochastic formation of magnetic vortex structures in asymmetric disks triggered by chaotic dynamics. *Nat. Commun.* **5**, 5620 (2014).

39. Brown, W.F. Thermal Fluctuations of a Single-Domain Particle. *Phys. Rev.* **130**, 1677-1686 (1963).

40. Shpyrko, O.G., Isaacs, E.D., Logan, J.M., Feng, Y., Aeppli, G., Jaramillo, R., Kim, H.C., Rosenbaum, T.F., Zschack, P., Sprung, M., Narayanan, S. & Sandy, A.R. Direct measurement of antiferromagnetic domain fluctuations. *Nature* **447**, 68-71 (2007).

41. Im, M.-Y., Fischer, P., Kim, D.-H., Lee, K.-D., Lee, S.-H. & Shin, S.-C. Direct Real-Space Observation of Stochastic Behavior in Domain Nucleation Process on a Nanoscale. *Adv. Mater.* **20**, 1750-1754 (2008).

42. Aron, Camille, Barci, D. G., Cugliandolo, L. F., Arenas, Z. G. & Lozano, G. S. Magnetization dynamics: path-integral formalism for the stochastic Landau-Lifshitz-Gilbert equation. *J. Stat. Mech.*, 09008-1-09008-59 (2014).

43. Kakazei, G. N., Ilyn, M., Chubykalo-Fesenko, O., Gonzalez, J. Serga, A. A., Chumak, A. V., Beck, P. A., Laege, B., Hillebrands, B. & Guslienko, K. Y. Slow magnetization dynamics and energy barriers near vortex state nucleation in circular permalloy dots, Appl. Phys. Lett. 99, 052512 (2011).

FIGURE LEGENDS

Figure 1. Magnetic imaging of asymmetrically shaped disks. Schematic diagram of asymmetric disks with a radius of R = 500 nm, a height of h = 100 nm, and an edge ratio of $r = 0.2R$ within an array with the interdisk distance of d = 200 nm. Representations of MTXM images of the in-plane magnetic components observed in a positive field sequence from +100 mT to 0 mT are inserted.

Figure 2. Controllability of circularity in asymmetric disk arrays with different geometries. (a) MTXM images of in-plane domain structures taken from four successive measurements by alternating the positive and negative field sequences in the disk arrays with R = 500 nm, h = 100 nm, and d = 200 nm. (b) Controllability of circularity by altering the direction of applied field investigated in disk arrays (R = 500 nm, d = 200 nm) with different edge ratios and disk heights. The values are obtained by the statistical analysis of generation probabilities of c in 1000 vortex formation events for each array. The error bar represents the standard deviation of controllability in 25 individual disks.

Figure 3. Simultaneous control of circularity and polarity in asymmetric disks. (a) MTXM images of in-plane and out-of-plane magnetic structures observed in identical region of the disk array (R = 500 nm, h = 100 nm, and $r = 0.2R$). (b) Simplified illustration of control of complete vortex structure, both c and p, by changing of direction of in-plane field.

Figure 4. Control of vortex structures by manipulation of stray field effect on dynamic process of vortex creation. (a) Series of snapshot images taken from simulations of vortex formation in isolated disk (upper) and in a disk within d = 201 nm array (lower). The disks are of $2R$ = 999 nm radius, h = 40 nm height, and r = 99 nm flat-edge ratio (~ $0.2R$). Here, the disks were immediately relaxed to 0 mT from a 100 mT saturation state without application of a control field. (b) Dynamic process observed by simulations, taking into account control fields of +10 mT and -10 mT additionally applied during the relaxation process of the isolated disk (upper) and the disk within the array (lower), respectively. The color on the disk surface corresponds to the curl of in-plane magnetization. The blue and red colors indicate the CW and CCW circularities, respectively.

Figure 5. MTXM images of finally formed circularities in the positive field sequence (+100 mT to 0 mT) without and with the control field of $H_{control}$ = +30 mT and -30 mT applied during vortex formation in an isolated disk (a) and in disks within array of d = 200 nm (b), respectively. The

dimensions of disks were $2R$ = 1 μm, h = 40 nm, r = 100 nm (~ 0.2R), which are almost equal to those ($2R$ = 999 nm, h = 40 nm, r = 99 nm (~ 0.2R)) of disk in simulations.

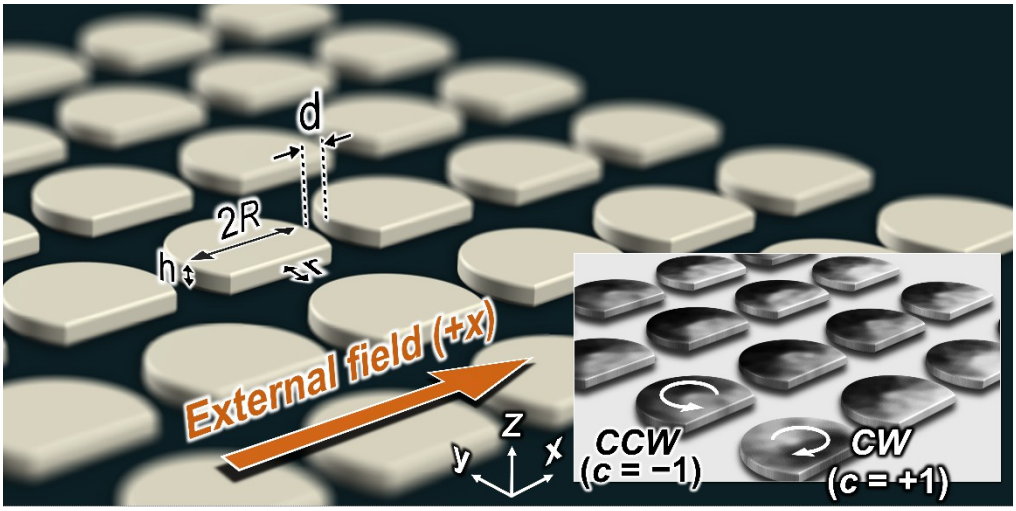

Fig. 1

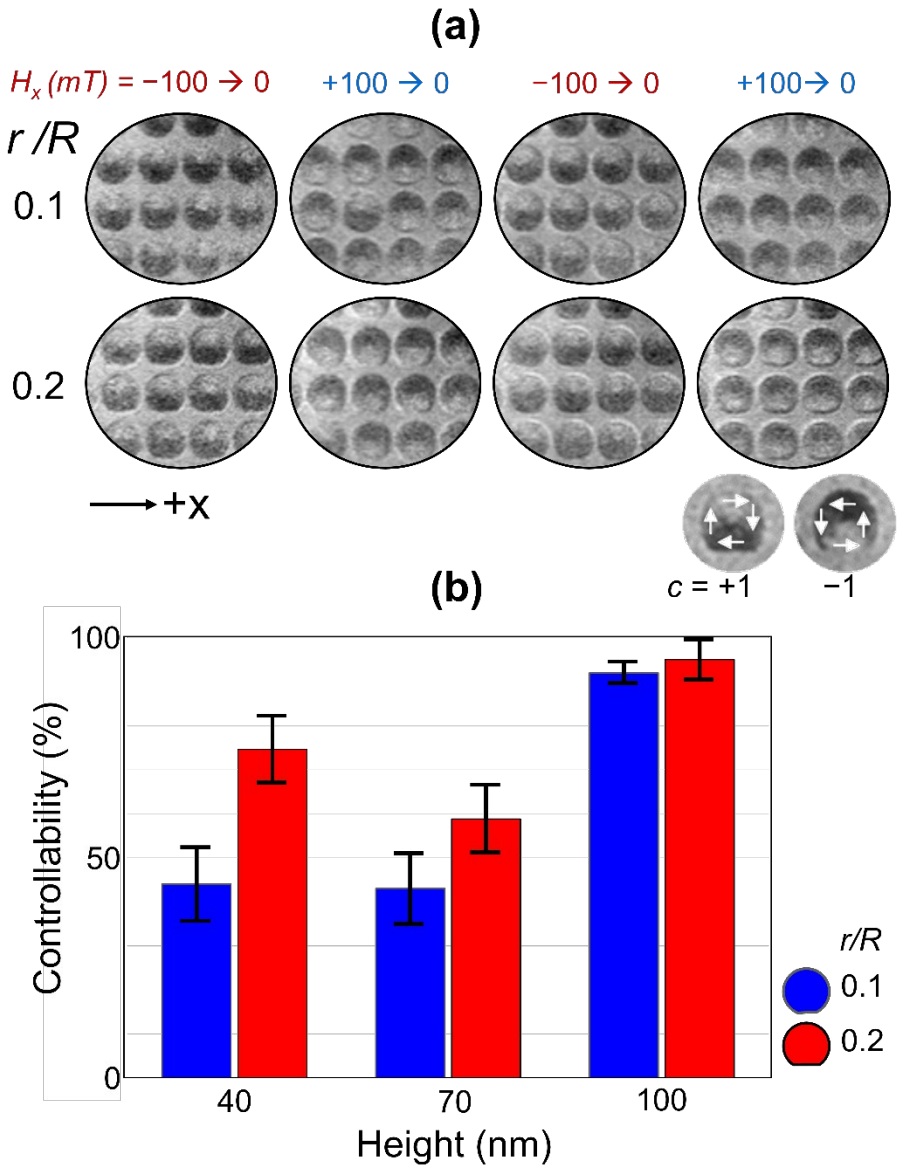
(a)
H_x (mT) = −100 → 0
+100 → 0
−100 → 0
+100→ 0
r /R
0.1
0.2
+x
c = +1
−1
(b)
Controllability (%)
100
50
0
40
70
100
Height (nm)
r/R
0.1
0.2

Fig. 2

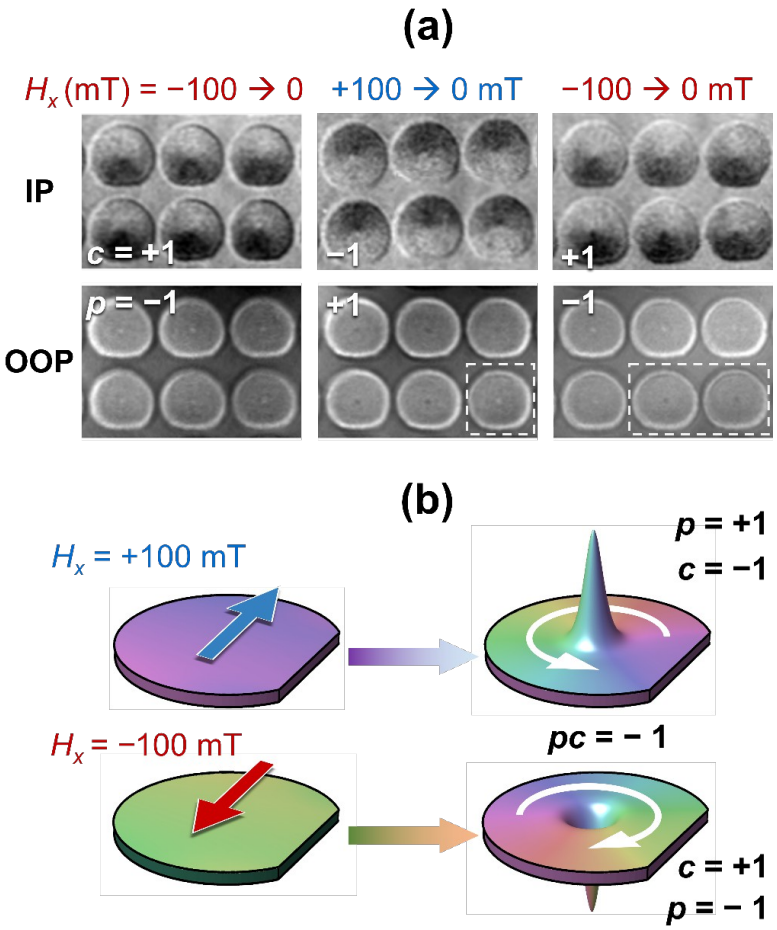
(a)
H_x (mT) = −100 → 0
+100 → 0 mT
−100 → 0 mT
IP
OOP
c = +1
−1
+1
p = −1
+1
−1
(b)
H_x = +100 mT
p = +1
c = −1
H_x = −100 mT
pc = − 1
c = +1
p = − 1

Fig. 3

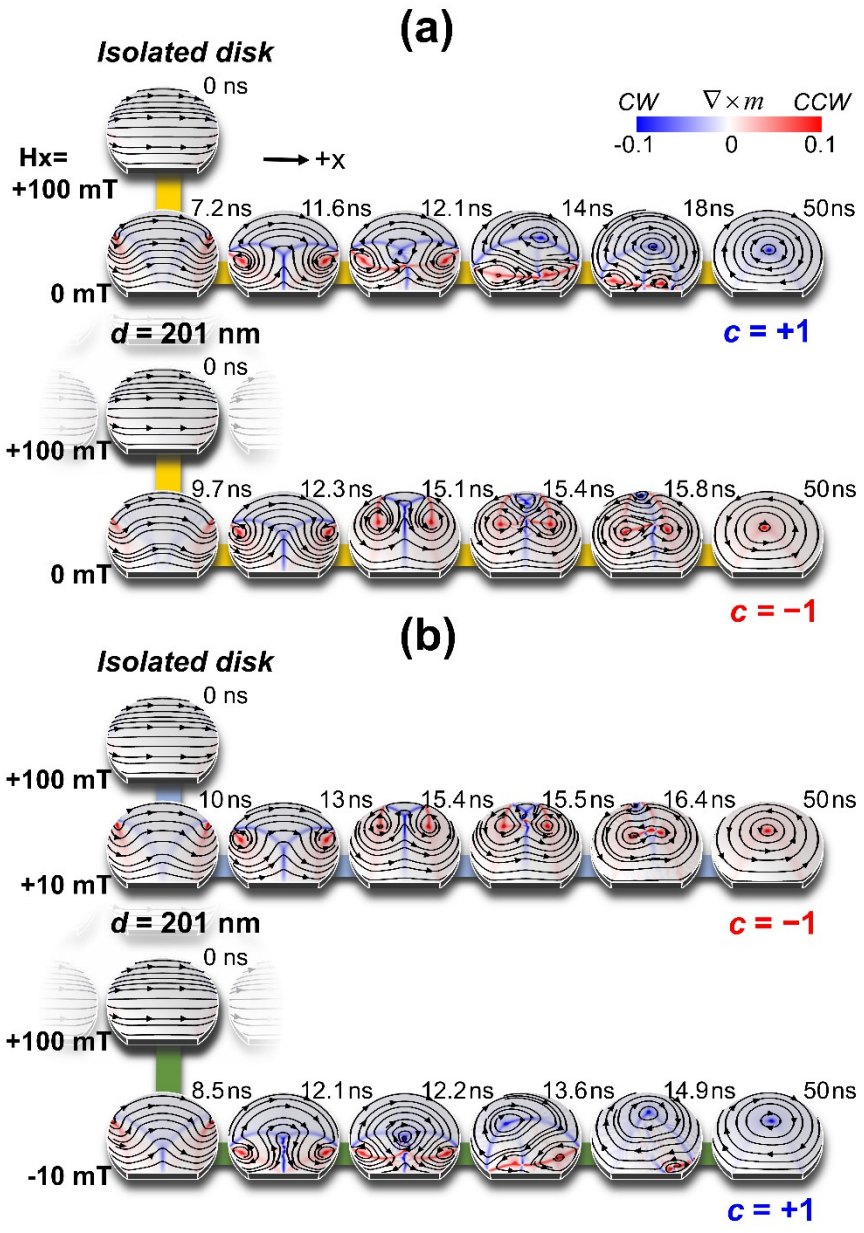
(a)
Isolated disk
0 ns
Hx=
+100 mT
+x
CW
∇×m
CCW
-0.1
0
0.1
7.2 ns
11.6 ns
12.1 ns
14 ns
18 ns
50 ns
0 mT
d = 201 nm
c = +1
0 ns
+100 mT
9.7 ns
12.3 ns
15.1 ns
15.4 ns
15.8 ns
50 ns
0 mT
c = −1
(b)
Isolated disk
0 ns
+100 mT
10 ns
13 ns
15.4 ns
15.5 ns
16.4 ns
50 ns
+10 mT
d = 201 nm
c = −1
0 ns
+100 mT
8.5 ns
12.1 ns
12.2 ns
13.6 ns
14.9 ns
50 ns
-10 mT
c = +1

Fig. 4

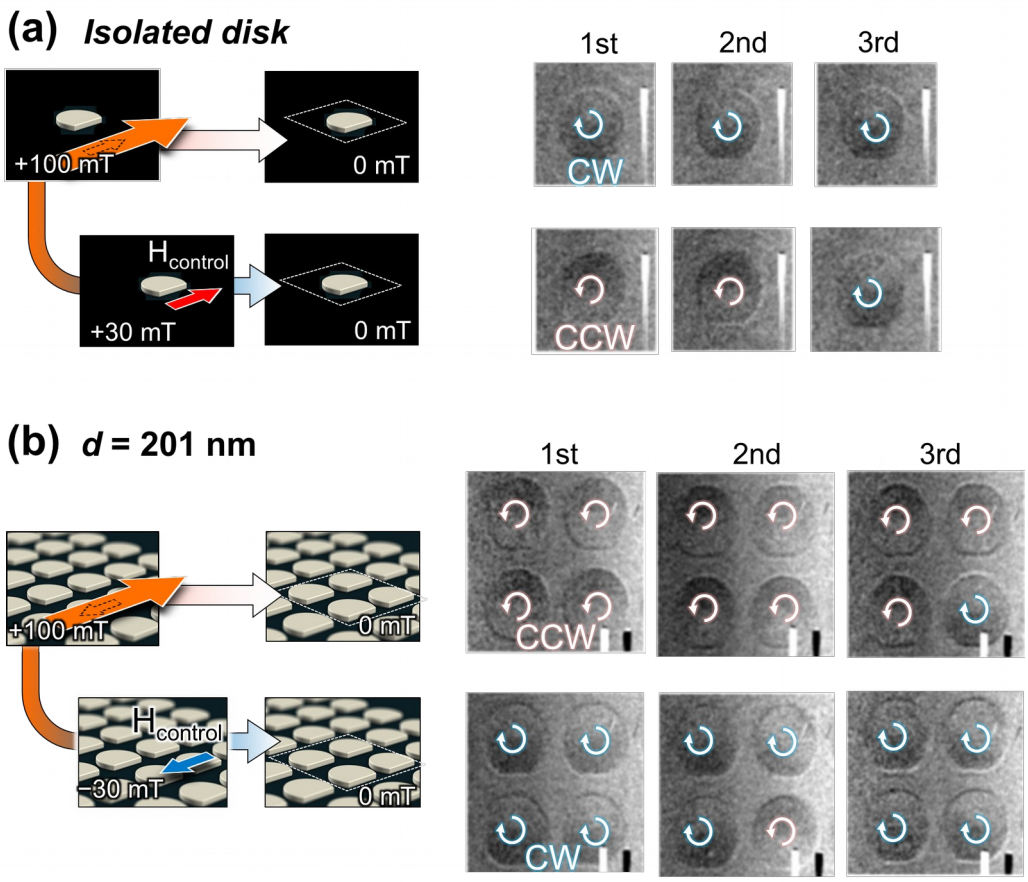
(a) Isolated disk
+100 mT
0 mT
H control
+30 mT
0 mT
1st
2nd
3rd
CW
CCW
(b) d = 201 nm
+100 mT
0 mT
H control
−30 mT
0 mT
1st
2nd
3rd
CCW
CW

Fig. 5